Geometrical resonances in the tunneling characteristics of superconducting Al films

Z. G. Khim and W. J. Tomasch
Department of Physics, University of Notre Dame, Notre Dame, Indiana 46556
(Received 24 April 1978)

Quasiparticle interference phenomena in thick Al films ($0.6 \leq d_1 \leq 3.1$ μm) backed by thin Pb ($d_2 \simeq 0.13$ μm) produce level structure which we employ to determine the dressed Fermi velocity v_F^* and the electron-phonon renormalization parameter Z_0 for films with pronounced [111] fiber textures. Although the proximity effect systematically enhances observed energy-gap values as Al-film thicknesses decrease, v_F^* and Z_0 remain constant at $(1.30 \pm 0.01) \times 10^6$ m/sec and 1.56. We infer a BCS coherence length of $\xi_0(\mathrm{Al}) = 1.54 \pm 0.05$ μm and a pairing potential decay length (at $T = 0.95$ K) of $K^{-1}(\mathrm{Al}) = 1.47 \pm 0.07$ μm. Values of the Pb energy gap inferred from virtual-state thresholds fall near the bulk average. Over the energy range investigated (0–7 meV), quasiparticles are not damped significantly by Pb phonon emission at the Al-Pb boundary.

I. INTRODUCTION

When two superconducting metals (M_1 and M_2) are brought into intimate contact, the resulting spatial change in the pairing potential ($\sim|\Delta_2 - \Delta_1|$) causes incident quasiparticles to suffer coherent Andreev reflections[1] at the M_1-M_2 interface. Andreev scattering in M_1, for example, corresponds to transitions between energetically degenerate states ($\omega^* = \omega = E - E_F$) lying just above and below the Fermi surface—that is, between states with $k^* \simeq k_F \pm (\omega^2 - \Delta_1^2)^{1/2}/\hbar v_F^*$, where v_F^* denotes the fully dressed Fermi velocity. In our experiment, M_1 is a thick Al film ($d_1 \sim 1$ μm) characterized by a reasonably long mean free path ($l_1 \sim d_1$) and M_2 is a thin Pb film ($d_1 \sim 0.1$ μm) deposited over one surface of M_1. For this geometry, interference effects involving incident and reflected portions of the quasiparticles are expected to contribute quasiperiodic level structure to the one-dimensional density of states $\rho_1(\omega, k_\perp)$ evaluated at the free surface of M_1 and, hence, to tunneling characteristics measured at this surface.[2-5] The approximate inverse dependence on film thickness exhibited by observed level spacings suggests quasiparticle standing waves established between the two surfaces of M_1. When Δ_2 exceeds Δ_1, as in the present case, levels with energies ω_n ($n = 1, 2, \ldots$) in the range $\Delta_1 < \omega_n < \Delta_2$ correspond to bound states, while those with $\omega_n \geq \Delta_2$ correspond to virtual states.[6] Our experiment basically consists of tunneling into M_1 with the aid of thin, superconducting Al counterelectrodes (CE) separated from the free surface by the usual natural oxide barrier. Comparisons between observed and computed tunneling characteristics are then employed to infer v_F^* and related quantities of interest

Wolfram's theory[5] for these geometrical resonances, based on an exact solution of the Gorkov equations for spatially constant energy gaps in M_1 and M_2, yields

$$\rho_1(\omega, k_\perp) = \mathrm{Re}\left[\rho_0(k_\perp)\frac{\omega}{\Omega_1}\left(1 + \frac{2(\Delta_1/\omega)\psi + 2\psi^2}{1 - \psi^2}\right)\right], \quad (1)$$

where

$$\psi(\omega) = re^{-\gamma}e^{2\pi i c\Omega_1} \quad (2)$$

is defined in terms of the reflection coefficient

$$r(\omega) = (R_1\Delta_2 - R_2\Delta_1)/(R_1R_2 - \Delta_1\Delta_2), \quad (3)$$

and where $k_\perp$ denotes the transverse component of momentum (which is actually directed parallel to all film surfaces). Other quantities appearing in Eq. (1) are defined according to

$$R_i = \omega + \Omega_i(\omega) \quad (i = 1, 2),$$
$$\Omega_i(\omega) = (\omega^2 - \Delta_i^2)^{1/2},$$
$$c = 2d_1/hv_F^*,$$
$$\gamma = 2d_1/l_1,$$

while $\mathrm{Re}[\rho_0(k_\perp)\omega/\Omega_1]$ corresponds to the unperturbed density of states. Since the condition $\psi^2 \ll 1$ is frequently satisfied—either because of damping associated with defect scattering ($\psi \propto e^{-\gamma}$), or because of decreasing $r \simeq (\Delta_2 - \Delta_1)/2\omega$ at higher energies—structure predicted by Eq. (1) can be frequently decomposed into two series of levels: one stemming from $(2\Delta_1/\omega)\psi$ and another from $2\psi^2$. These have asymptotic level spacings of $hv_F^*/2d_1$ and $hv_F^*/4d_1$, respectively, and will be referred to as the $2d$ and $4d$ series. Clearly, defect scattering not only controls the overall scale of structure via $\psi \simeq (|\Delta_2 - \Delta_1|/2\omega)e^{-\gamma}$, but also the relative importance of the two series, since at higher energies $|2\psi^2|/|(2\Delta_1/\omega)\psi| \simeq (|\Delta_2 - \Delta_1|/2\Delta_1)e^{-\gamma}$. For strong damping ($\gamma > 3.7$) only the $2d$ series is resolved, while for weaker damping both are resolved and the

level spacing decreases from $hv_F^*/2d_1$ to $hv_F^*/4d_1$. In the latter instance, level amplitudes frequently alternate in strength because of interference, giving rise to the so-called strong-weak (SW) effect.[8] Comparisons between tunneling characteristics computed utilizing Eq. (1) and those observed with films of known thickness permit precise and reliable experimental determinations of v_F^* and the renormalization function $Z(\omega=0)=Z_0=v_{F0}/v_F^*=1+\lambda$ evaluated at the Fermi surface, where v_{F0} and λ denote the bare band velocity and the electron-phonon coupling strength, respectively. Procedures employed to compute characteristics for tunneling between two superconductors are outlined in Appendix A.

Achieving adequate level amplitudes with evaporated Al films presents a challenge because of practical mean-free-path limitations. Unlike softer metals, Al films manufactured by the methods of Sec. II rarely exhibit values of l_1 in excess of ~1.5 μm.[7] Since amplitudes scale as $\psi \simeq (|\Delta_2-\Delta_1|/2\omega)e^{-\gamma} \propto |\Delta_2-\Delta_1|$, realization of useful level structure requires use of large gap perturbations. Pb overlayers prove nearly ideal in that they provide substantial perturbations [Δ_0(bulk Pb) $-\Delta_0$(bulk Al) $\simeq 1.36-0.14$ meV $\sim 9\Delta_0$(bulk Al)] without introducing noticeable metallurgical problems which could in of themselves prevent the occurrence of level structure. We have, therefore, utilized junctions of the form Al–AlO_x–Al(M_1)–Pb(M_2) to measure v_F^* and Z_0. As we shall see, agreement between observed tunneling structure and that computed from the weak-coupling form of Wolfram's theory (Δ_2 = const) is quite good for $\gamma > 3.5$; otherwise, strong-coupling effects in Pb must be included via $\Delta_2 = \mathrm{Re}[\Delta_{Pb}(\omega)] + i\,\mathrm{Im}[\Delta_{Pb}(\omega)]$ before good agreement is restored.

We have devoted considerable attention to evaluating $I(V)$ characteristics (Sec. III) for a substantial number of junctions and analyzing the inferred gap values for possible clues as to the overall quality of the Al crystallites probed by tunneling. Our $I(V)$ characteristics and gap values generally resemble those obtained previously by tunneling into films and bulk single crystals. (On rare occassions, approximately 4% of the time, we also observe two resolved energy gaps differing by 5%–10%.) Taken all together, x-ray evidence, measured level amplitudes, and energy-gap values suggest tunneling from high-quality Al(M_1) crystallites having strong [111] textures and mean free paths as long as ~1.5 μm.

II. EXPERIMENTAL METHODS

An oil-pumped conventional vacuum station (glass–Viton–stainless-steel) equipped with water- and nitrogen-cooled baffles provided pressures in the range $8\times10^{-8} \leq P \leq 8\times10^{-7}$ Torr. All metal evaporations were conducted using resistively heated sources: triple-stranded W baskets for Al; Mo boats for Pb. Evaporation rates typically fell in the ranges ~300–500 Å/sec for Al and 40–100 Å/sec for Pb. Although only 99.9%-purity Pb was used for overlayers in an attempt to limit l_2, 99.999%-purity Al material was used for all Al films, including the thin (~0.1 μm) counterelectrodes employed. Natural-oxide tunnel barriers grown on these counterelectrodes by exposure to air were subsequently masked with Formvar varnish to preclude tunneling from any film edges. Only minimal delays (~10–20 sec) occurred between Al(M_1) and Pb(M_2) evaporations so as to reduce potential contamination of the Al-Pb interface. Approximately 15 min were required to transfer newly completed junctions to a ^{4}He cryostat prior to cooling to $T \simeq 77$ K. A vibrating quartz-crystal monitor provided initial thickness estimates during film fabircations, while final thicknesses were determined either by Michelson interferometer ($d_1 > 1$ μm) or Tolansky interferometer ($d_1 \leq 1$ μm) after coating the entire substrate with Al (~0.1 μm). Ordinary glass microscope slides served as substrates for all junctions. X-ray diffractometer studies carried out with films of larger area, deposited by similar methods, confirmed pronounced [111] fiber textures in both Al and Pb films, although indications of a much weaker [101] Al texture were seen in some instances.

A conventional bridge spectrometer, patterned after the design of Adler and Jackson[9] and operated in the current modulation mode, supplied traces of dV/dI and d^2V/dI^2 as continuous functions of dc bias V. Quoted modulation levels (μV, rms) refer to biases substantially above the sum-of-gaps potential $V_B = (\Delta_{CE}+\Delta_1)/e$ and, hence, are much larger than modulation levels pertaining near V_B.

III. dc TUNNELING

Of 56 junctions tested ($0.90 \leq T \leq 1.15$ K), 48 produced acceptable $I(V)$ characteristics dominated by single-particle tunneling; and of these, 46 yielded traces similar to curve (a) of Fig. 1, while two others yielded traces similar to curve (b). Characteristics typified by curve (a) approximate those anticipated for $\Delta_1 = \Delta_{CE}$ and generally resemble results reported by Blackford and March[10] for thinner films at comparable temperatures, although the latter films exhibited somewhat sharper current increases near $V_B = (\Delta_{CE}+\Delta_1)/e$. This broadening of the current rise is due in part to the influence exerted by the first bound state which, by

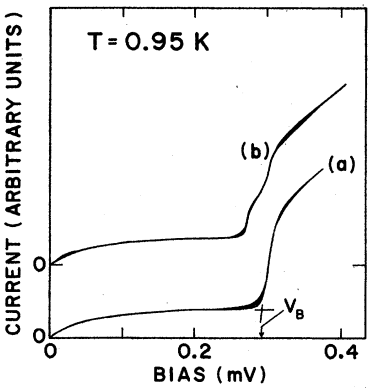

FIG. 1. dc tunneling characteristics. Trace (a) approximates $I(V)$ behavior anticipated for two superconductors having energy gaps which are nearly equal ($\Delta_{CE} \approx \Delta_1$) and is representative of results obtained with 46 junctions. Trace (b) suggests a second gap in M_1 and is representative of two junctions. Computed fits based on Wolfram's theory are also plotted; areas between observed and computed traces have been filled in, causing the trace broadenings apparent in the figure. Experimental values of $V_B = (\Delta_{CE} + \Delta_1)/e$ are obtained by the extrapolation method. [Parameter values employed for fitting (a) are $\Delta_{CE} = 0.140\ (1 + 0.02i)$ meV, $\Delta_1 = 0.156\ (1 + 0.02i)$, $\Delta_2 = 1.40$, $c = 0.742$ meV^{-1}, $\gamma = 4.00$, and $T = 0.95$ K; for (b) $\Delta_{CE} = 0.130\ (1 + 0.02i)$, $\Delta_1' = 0.174(1 + 0.02i)$ with Δ_1, Δ_2, c, γ, and T as before.]

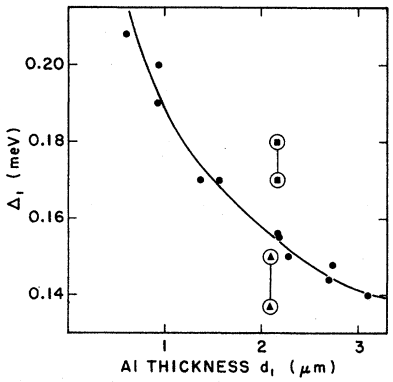

FIG. 2. Energy-gap values ($T = 0.95$ K) inferred from $I(V)$ characteristics of the 13 junctions utilized to determine v_F^*. Two junctions exhibit double gaps.

Eq. (1), depresses $\rho_1(\omega, k_\perp)$ at the gap edge according to $\rho_1(\Delta_1, k_\perp)/\rho_0(k_\perp) = \tanh\frac{1}{2}\gamma$, causing 5%–10% effects ($3 \leq \gamma \leq 4$) in most of our junctions. On the otherhand, bulk Al single crystals[11] also yield $I(V)$ characteristics which resemble curve (a), including gradual current increases at V_B.

Trace (b) differs from (a) in that the current increase ordinarily associated with V_B appears to be repeated a second time at a slightly different bias. Campbell and Walmsley have interpreted similar behavior, observed with a thick[12] polycrystalline film, in terms of two distinct energy gaps. Their small gap is quite comparable to the values we observe with either type junction [trace (a) or (b)], but their second gap is roughly twice as large as any we have encountered. Our use of thin Al counterelectrodes ($d_{CE} \ll \xi_0$) presumably precludes occurrence of multiple gaps in these films, while masking both sets of edges prevents tunneling from potentially atypical edge regions. In view of these precautions, we also interpret traces like (b) in terms of two energy gaps having comparable strengths in the sense of producing comparable structure in $I(V)$.

The polycrystalline nature of our films raises a question with regard to traces like (b): Do individual crystallites exhibit two energy gaps, or are two crystallite populations involved, each characterized by a different energy gap? Blackford's single-crystal tunneling studies[11] do not support the coexistance of two prominent energy gaps for any orientation, although some junctions apparently evidenced weak structure in dV/dI which might indicate a very weak second gap. His observations do indicate substantial crystalline anisotropy (~±17%), however, enough to easily accommodate the gap variations (~±10%) exhibited by our two atypical junctions. It seems more likely, therefore, that traces like (b) result from some chance occurrence—such as preferential tunneling from a large, atypically oriented crystallite, or realization of an unusually strong minority texture—rather than from two intrinsic energy gaps whose observation might, for example, signal uncommonly good film quality.

Twenty-three junctions with acceptable $I(V)$ characteristics also exhibited some degree of level structure in d^2V/dI^2, and 13 of these (including the two atypical junctions) evidenced sufficient structure to warrant their use in determining v_F^*. Values of Δ_1 for these 13 junctions appear in Fig. 2 as a function of thickness.[13] As anticipated, thinner films display modest gap enhancements due to proximity effect. The two instances involving double energy gaps—falling, as they do, either entirely above or entirely below the smooth curve—fail to suggest a trend. To enable comparisons with previous work,[10-12] one would like to extract a gap estimate $\Delta_1(\infty) = \Delta_1(d_1 \to \infty)$ which characterizes our films when proximity effects are absent, and which utilizes as much available information as possible. Figure 3 presents a plot of $\ln[\Delta_1(d_1) - \Delta_1(\infty)]$ vs d_1 for the 11 single-gap junctions of Fig. 2, where the value $\Delta_1(\infty) = 0.127$ meV employed yields the best least-squares fit. Figure 3 demonstrates that observed gap variations are described quite well by $\Delta_1(d_1) = \Delta_1(\infty) + \delta\Delta \exp(-d_1/K^{-1})$, where

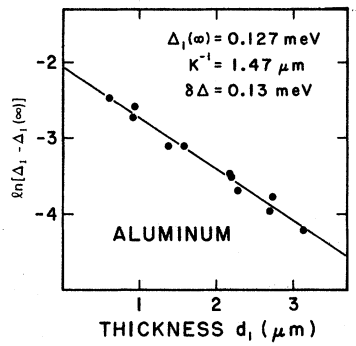

FIG. 3. Semilogarithmic plot of gap enhancements vs film thickness for the 11 single-gap junctions of Fig. 2.

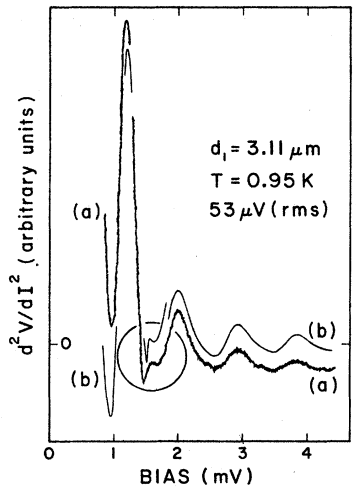

FIG. 4. Observed (a) and computed (b) second derivatives for the thickest Al film studied. The generally good agreement between (a) and (b) extends through the virtual-state threshold $V = (\Delta_2 + \Delta_{CE})/e$ (encircled), permitting precise determinations of the parameter Δ_2 in Wolfram's theory. Observed values $\Delta_2 = 1.40 \pm 0.02$ meV differ but little from that of bulk Pb. Segments of (b) have been displaced vertically for clarity. [Parameters employed for (b) are $\Delta_{CE} = 0.166(1 + 0.05i)$, $\Delta_1 = 0.150(1 + 0.05i)$, $\Delta_2 = 1.38$, $c = 1.00$, $\gamma = 4.00$, $\beta = 30$, $T = 0.95$ K and 53-μV modulation.]

K^{-1} denotes the pairing potential decay length determined by the slope of Fig. 3. The inferred value $K^{-1} = 1.47 \pm 0.07\ \mu$m falls near $K_0^{-1} = \hbar v_F^*/2\pi k_B T = 1.62 \pm 0.05\ \mu$m expected for a clean normal metal ($\lambda = 0$), but is noticeably smaller than the coherence length $\xi(T) = 2.3\ \mu$m estimated for a clean superconductor ($T_c = 1.23$ K) using $\xi(T) = 0.74\xi_0(1 - T/T_c)^{-1/2}$, where ξ_0 is the BCS coherence length determined in Sec. V.

The values of $\Delta_1(\infty)$ inferred at $T \simeq 0.95$ K corresponds to a zero-temperature BCS value $\Delta_0(\mathrm{Al}) = 0.177 \pm 0.07)$ meV, in reasonably good accord with the Blackford and March[10] result ($\Delta_0 = 0.186$ meV), as well as with the smaller of the Campbell and Walmsley results ($\Delta_0 = 0.17$ meV).[12] Rapid variations in Blackford's single-crystal values of Δ_0 frustrate comparisons between his work[11] and ours. Moving ~6° off [111], for example, causes Δ_0 to increase from 0.150 to 0.200 meV, while moving to another orientation ~12° off [111] restores Δ_0 to 0.150 meV—variations which span the maximum range of his observations.[11] Even for sharply peaked [111] fiber textures, these results may be interpreted so broadly ($0.150 \leq \Delta_0 \leq 0.200$ meV) as to be of marginal value in assessing crystallite quality. We can say only that our limiting value of Δ_0 is compatible with tunneling from high-quality crystallites having a strong [111] texture.

Theoretical $I(V)$ characteristics obtained from computations based on Wolfram's density of states are also plotted in Fig. 1. These computations take into account effects due to nonzero temperature, angular dependence of the tunneling matrix element (via β),[14] and residual gap smearing. As a practical matter, any successful calculation of $I(V)$ must provide for a certain amount of gap smearing, even when $I(V)$ rises rapidly near V_B. Following Wyatt, Barker and Yelon,[15] we simulate residual smearing (both in M_1 and CE) by replacing Δ (a real constant) in the BCS formula $\rho = \mathrm{Re}[\rho_0(k_\perp)\omega/(\omega^2 - \Delta^2)^{1/2}]$ with $\Delta(1 + i\delta)$—that is, by adding a small imaginary constant ($\delta \ll 1$) to Δ—which removes the discontinuity in ρ at $\omega = \Delta$, adds states in the gap region ($0 \leq \omega < \Delta$) and, to a very good approximation, preserves normalization.[15] According to Fig. 1, $I(V)$ characteristics computed for reasonable parameter values are in excellent agreement with those actually observed.

IV. ac TUNNELING

Second-derivative data acquired with the thickest Al film studied ($d_1 = 3.11\ \mu$m) appear in Fig. 4. The low modulation level employed yields a poor signal at higher biases (energies), but preserves structural detail which occurs at lower biases. Estimates based on normalized first-derivative amplitudes suggest a value of $\gamma = 4.0$, so that $2d$ amplitudes should exceed $4d$ amplitudes by a factor of approximately 12 [$|2\psi^2|/|(2\Delta_1/\omega)\psi| \simeq (|\Delta_2 - \Delta_1|/2\Delta_1)e^{-\gamma} \simeq \frac{1}{12}$], precluding resolution of the $4d$ series and fixing the basic level spacing at $hv_F^*/2d_1$. Agreement between observed and predicted second derivatives—the latter computed for $\gamma = 4.0$—is seen to be quite satisfactory (Fig. 4), extending even to subtle details such as sawtooth line shapes ($2 \leq \omega = eV - \Delta_{CE} \leq 3.5$ meV) and fine structure near $\omega = \Delta_2$. Data acquired with larger modulations exhibit virtual-state oscillations which extend to ω

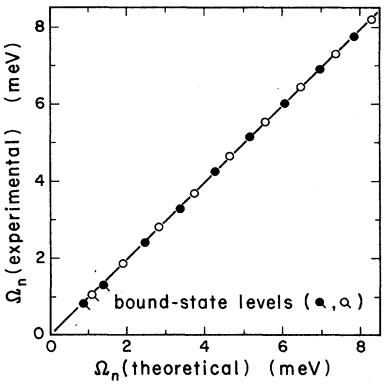

FIG. 5. Observed level locations plotted against predicted locations for the junction of Fig. 4. Both dips (●) and peaks (○) in d^2V/dI^2 are plotted. The 45° line included in the figure corresponds to perfect agreement between experiment and theory.

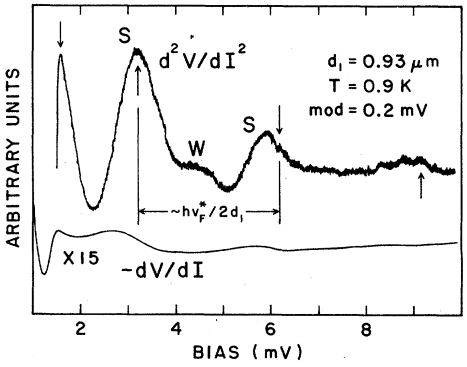

FIG. 7. Observed level structure for a comparatively thin Al film. Vertical arrows mark anticipated $2d$ level locations (S), computed from d_1 and v_F^* (thick-film value), assuming Δ_2 does not vary with energy. The dotted curve of Fig. 8 gives the actual structure predicted by this calculation.

$\simeq 8$ meV and which allow a further test of the theory by plotting observed values of Ω_n (corresponding to peaks or dips in d^2V/dI^2) against predicted values, as shown in Fig. 5. The 45° straight line obtained indicates excellent agreement and permits precise determination of $c = 2d_1/hv_F^*$ (hence, of v_F^* itself) since only one value of c can yield the good agreement depicted.

First and second derivatives presented in Fig. 6 exhibit somewhat stronger structure corresponding to $\gamma = 3.4$. This time $2d$ amplitudes exceed $4d$ amplitudes by a factor of approximately 8, yielding a partially resolved $4d$ series. Agreement is again quite good, reaffirming one's confidence in the theory and in the basic level spacing assignment $hv_F^*/2d_1$.

Further decreases in γ, achieved by decreasing d_1, produce level structure which is not only stronger—but which also has a different general appearance, as shown in Fig. 7. Comparisons of observed and computed tunneling characteristics help focus attention on these differences. The required computations pose no problem since three of the parameters needed are known with considerable precision [c from the thick-film average of v_F^* and direct measurements of d_1; Δ_1 (=const) from $I(V)$; and Δ_2 (=const) from the virtual-level threshold in d^2V/dI^2], while the fourth (γ) can be estimated from normalized first-derivative ampli-

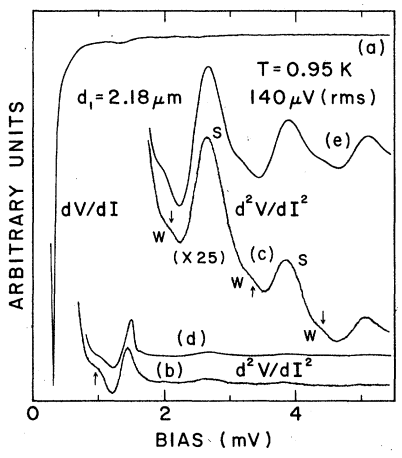

FIG. 6. Partially resolved $4d$ structure observed with an Al film of intermediate thickness. Levels of the $4d$ series are indicated by arrows and labeled W (weak), while $2d$ levels are labeled S (strong). Curves (a)–(c) represent experimental traces; (d) and (e) represent computed quantities corresponding to (b) and (c), respectively. [Parameters employed for (c) and (d) are $\Delta_{CE} = 0.130(1+0.05i)$, $\Delta_1 10.170(1+0.05i)$, $\Delta_2 = 1.41$, $c = 0.831$, $\gamma = 3.4$, $\beta = 30$, $T = 0.95$, and 140-μV modulation.]

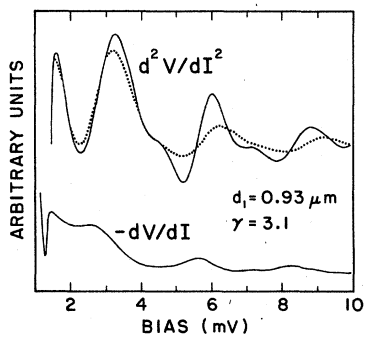

FIG. 8. Computed derivative structure for the junction of Fig. 7. Computations based on Wolfram's theory with Δ_2 held constant yield the dotted curve, while similar computations with $\Delta_2(\omega) = \mathrm{Re}[\Delta_{Pb}(\omega)] + i\mathrm{Im}[\Delta_{Pb}(\omega)]$ yield the solid curves. [Parameters employed are: $\Delta_{CE} = 0.130(1+0.05i)$, $\Delta_1 = 0.190(1+0.05i)$, $\Delta_2 = 1.40$, $c = 0.345$, $\gamma = 3.1$, $k_\perp = 0$, and $T = 0$.]

tudes. Results computed on this basis appear as the dotted curve of Fig. 8, and comparison with Fig. 7 shows that the observed $4d$ structure (labeled W) is much stronger than predicted; furthermore, dominant peaks observed at higher biases are displaced from their predicted locations. In general, therefore, Wolfram's theory in its weak-coupling form is unable to provide an adequate account of our observations with thinner Al films ($0.6 \leq d_1 \leq 1.0$ μm).

Good agreement can be restored, however, by including strong-coupling effects in the overlayer, that is, by relaxing the approximation $\Delta_2 = \text{const}$ and permitting $\Delta_2(\omega) = \text{Re}[\Delta_2(\omega)] + i\,\text{Im}[\Delta_2(\omega)]$ to assume the correct functional form describing Pb. Some insight into why this should be so can be gained by noting that the relative importance of the $4d$ contribution varies as $|2\psi^2|/|(2\Delta_1/\omega)\psi| \simeq [|\Delta_2(\omega)|/2\Delta_1]e^{-\gamma}$, and that $|\Delta_2(\omega)| = |\Delta_{\text{Pb}}(\omega)|$ experiences large increases (~4×) near peaks in the phonon density of states which occur at $\omega_T \simeq 4.5$ meV and $\omega_L \simeq 8.5$ meV. Of course, the fact that $|2\psi^2|/|(2\Delta_1/\omega)\psi|$ scales as $e^{-\gamma}$ explains why decreasing γ values emphasize effects due to $\Delta_2(\omega)$. Repeating our previous calculations for d^2V/dI^2—but now with complex value of $\Delta_2(\omega) = \Delta_{\text{Pb}}(\omega)$ taken from the compilation of Rowell, McMillan, and Dynes[16]—we obtain the solid curve of Fig. 8. Comparison of Figs. 7 and 8 shows that agreement has been restored; level amplitudes and displacements, the latter given by $(1/2\pi c)\arctan\{\text{Im}[\Delta_2(\omega)]/\text{Re}[\Delta_2(\omega)]\}$, are both accounted for. Inverting this procedure, in the sense of inferring parameter values from theoretical fits to observed structure obtained with (three) thinner films ($0.6 \leq d_1 \leq 1.0$ μm), yields values of v_F^* which fall within 1% of the thick-film average. For these films, variations in $\Delta_2(\omega)$ also influence the decrease of $2d$ and $4d$ level amplitudes with increasing energy ($\omega = eV - \Delta_{\text{CE}}$) since $|\psi(\omega)|$ varies as $|\psi| \simeq [|\Delta_2(\omega) - \Delta_1|/2\omega]e^{-\gamma} \simeq [|\Delta_2(\omega)|/2\omega]e^{-\gamma}$ at higher energies, yielding $2d$ and $4d$ amplitudes in $\rho_1(\omega, k_\perp)$ which decrease as $\Delta_1|\Delta_2(\omega)|(1/\omega^2)e^{-\gamma}$ and $|\Delta_2(\omega)|^2(1/2\omega^2)e^{-2\gamma}$. The occurrence of sizable effects due to changes in $\Delta_2(\omega)$ requires somewhat special circumstances: M_2 must be strong coupling, of course, and defect scattering in M_1 must not be too strong—but, also, level amplitudes must not be quenched by spontaneous phonon emission in M_1 at energies below those for which $\Delta_2(\omega)$ increase substantially. Hence, M_1 should have its first phonon peak at a significantly higher energy [$\omega_T(\text{Al}) \simeq 20$ meV] than that of M_2 since spontaneous phonon emission can be quite effective in quenching level structure even in weak-coupling superconductors.

Returning to thicker Al films ($\gamma > 3.5$), where effects due to $\Delta_2(\omega)$ are negligible, Wolfram's theory predicts amplitudes for $\rho_1(\omega, k_\perp)$ which decay as $1/\omega^2 \simeq 1/\Omega_1^2$ at higher energies. For specular tunneling ($k_\perp/k_F = \sin\theta \simeq 0$), numerical computations show this prediction carries over to d^2V/dI^2. For random tunneling, where all tunneling directions are assumed equally likely, numerical computations show that Wolfram's theory leads to a $1/\omega^3 \simeq 1/\Omega_1^3$ decay for d^2V/dI^2. Following McMillan,[17] we parametrize the tunneling matrix element (squared) according to $\beta\exp(-\beta\theta^2/2) \simeq \beta e^{-\beta} \times e^{\beta\cos\theta}$, so that behavior intermediate between these two limits can be realized by adjusting β.[14] Second-derivative amplitudes obtained with an Al film exhibiting only $2d$ levels ($\gamma = 4.0$) appear plotted as a function of Ω_1 in Fig. 9. Dashed curves representing the specular and random tunneling limits are included for comparison. The actual decay law falls between these two extremes and, over the interval 2.5–7 meV, can be fit quite well by $\beta = 30$, a choice[18] which corresponds to an rms tunneling angle of about 15°. Accelerated amplitude decays observed at higher energies probably indicate the onset of significant damping by spontaneous phonon emission in Al. An interesting aspect of these results is the absence of any additional damping above $\omega_T(\text{Pb}) \sim 4.5$ meV, indicating that quasiparticles incident upon the Al-Pb interface from the

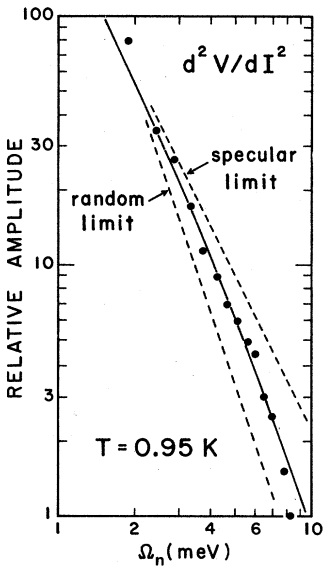

FIG. 9. Decay of $2d$ amplitudes in d^2V/dI^2 for the junction of Figs. 4 and 5. The solid curve corresponds to the theoretical prediction for $\beta = 30$. Absence of enhanced damping above $\omega_T(\text{Pb}) \simeq 4.5$ meV demonstrates the absence of Al quasiparticle damping by emission of transversely polarized Pb phonons during encounters with the Al-Pb interface. Accelerated amplitude decay above 7 meV probably results from spontaneous emission of Al phonons, although longitudinally polarized Pb phonons can not be ruled out since $\omega_L(\text{Pb}) \simeq 8.5$ meV.

Al side are not scattered inelastically by emission of transversely polarized Pb phonons even though such events are energetically permitted.

V. NUMERICAL RESULTS AND COMPARISONS

Values of v_F^* ([111]) inferred by matching computed and observed second derivatives for three thin films ($0.6 \leq d_1 \leq 1.0$ μm) and ten thick films ($1.0 < d_1 \leq 3.1$ μm) are presented in Fig. 10. Absence of any systematic trend in v_F^* with decreasing thickness—and, hence, with increasing gap enhancement—demonstrates the insensitivity of Z_0 to proximity-effect phenomena, at least on the scale of effects encountered in our experiment. Also, because of the smallness of the intrinsic gap in Al, Z_0 values for the normal and superconducting states should be very nearly equal. Adopting the plausible interpretation that scatter in our velocity determinations (characterized by a standard deviation of 0.04×10^6 m/sec) is due primarily to random errors in the measurement of d_1, we obtain the value $v_F^*([111]) = (1.30\pm0.01)\times10^6$ m/sec, a result which compares favorably with the specific heat value (1.27×10^6 m/sec) due to Daunt[19] and the anomalous skin-effect value (1.29×10^6 m/sec) due to Fawcett.[20] Combining this result with the value $v_{F0}([111]) = 2.03\times10^6$ m/sec inferred from the pseudopotential fit of the Fermi surface by Anderson and Lane[21] (based on de Haas–van Alphen measurements), we obtain $Z_0([111]) = v_{F0}/v_F^* = 1.56$, or $\lambda([111]) = 0.56$—in fair agreement with theoretical estimates by Allen and Cohen[22] ($\lambda = 0.53$) and by Ashcroft and Wilkins[23] ($\lambda = 0.49$), but substantially larger than the emperical estimate ($\lambda = 0.38$) by McMillan.[24] Finally, v_F^* and Δ_0(Al) can be combined to yield a BCS coherence length $\Delta_0(\mathrm{Al}) = \hbar v_F^*/\pi\Delta_0 = 1.54\pm0.05$ μm which falls remarkably close to the decay length $K^{-1} = 1.47\pm0.07$ μm inferred from Fig. 3.

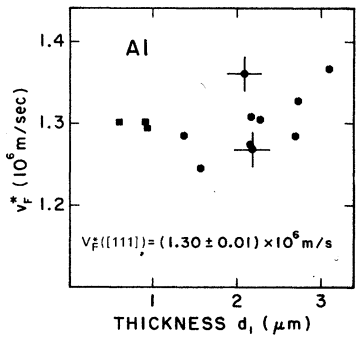

FIG. 10. Values of v_F^* ([111]) as a function of Al film thickness. Velocities marked by crosses correspond to values obtained with two a typical junctions exhibiting double energy gaps. The presence of two gaps appears to have no effect on v_F^*.

ACKNOWLEDGMENT

This work was supported by NSF Grant No. DMR76-16998.

APPENDIX A: COMPUTATION OF TUNNELING CHARACTERISTICS FROM WOLFRAM'S THEORY

Assuming the tunneling matrix element $T(k_\perp)$ depends only on transverse momentum $k_\perp = k_F \sin\theta$—where θ denotes the tunneling direction relative to the barrier normal—the current passing between two superconductors ($T = 0$ K) due to an applied bias V can be written as[5]

$$I(V) \propto \int_{-\infty}^{\infty} d\omega \int_0^{k_F} \frac{d^2k_\perp}{(2\pi)^2} |T(k_\perp)|^2 \times \rho_{CE}(\omega', k_\perp)\rho_1(\omega, k_\perp)$$
$$\propto \int_{-\infty}^{\infty} d\omega\, \rho_{CE}(\omega', 0) \int_0^{k_F} \frac{d^2k_\perp}{(2\pi)^2} \left|\frac{T(k_\perp)}{T(0)}\right|^2 \times \left[\frac{\rho_{CE}(\omega', k_\perp)}{\rho_{CE}(\omega', 0)}\right] \rho_1(\omega, k_\perp), \tag{A1}$$

with $\omega' = eV - \omega$ and $d^2k_\perp = 2\pi k_\perp dk_\perp = 2\pi k_F^2 \sin\theta\cos\theta\, d\theta$. For a counterelectrode having completely isotropic electronic properties,

$$\rho_{CE}(\omega', k_\perp) = \frac{m}{\pi\hbar k_F^2 \cos\theta} \mathrm{Re}\left(\frac{\omega'}{[(\omega')^2 - \Delta_{CE}^2(\omega')]^{1/2}}\right), \tag{A2}$$

where the prefactor containing $\cos\theta$ corresponds to $\rho_{CE}(\omega', k_\perp) = \rho_0(k_\perp)$ in the normal state [$\Delta_{CE}(\omega') = 0$] and where $\Delta_{CE}(\omega')$ could, in principle, be a complex function of energy. The current now simplifies to

$$I(V) = K \int_{-\infty}^{\infty} d\omega\, \rho_{CE}(\omega', 0) \times \int_0^{\pi/2} D(\theta)\rho_1(\omega, \theta)\sin\theta\, d\theta, \tag{A3}$$

where K is a constant and $D(\theta) = |T(\theta)/T(0)|^2$. This result is easily extended to nonzero temperatures by introducing the usual Fermi-Dirac functions [e.g., $f(\omega, T)$] in the energy integration via the factor $F(\omega, \omega', T) = f(\omega, T) - f(\omega', T)$.

In the extreme specular limit—where θ is restricted to vanishingly small values and all electrons tunnel normal to the barrier—$D(\theta)\sin\theta$ assumes δ-function character and Eq. (A3) reduces to the so-called semiconductor result,

$$I(V) = K \int_{-\infty}^{\infty} d\omega F(\omega, \omega', T) \times \rho_{CE}(\omega', 0)\rho_1(\omega, 0), \tag{A4}$$

involving the familiar convolution integral of two one-dimensional densities of states. To improve upon this result by permitting reduced rates of tunneling for $\theta > 0$, one must adopt a model for the barrier in the sense of specifying the barrier transmission function $D(\theta)$. A Gaussian variation $D(\theta) = \beta \exp(-\beta\theta^2/2)$ proves a particularly tractable choice.[17] The parameter β is related to the rms tunneling (half) angle

$$\langle\theta\rangle = \left(\int_0^{\pi/2} \theta^2 D(\theta) \sin\theta \, d\theta\right)^{1/2} \tag{A5}$$

according to

$$\langle\theta\rangle = (2/\beta)^{1/2}(1-\beta e^{-\beta})^{1/2} \approx (2/\beta)^{1/2}, \tag{A6}$$

so that a value of $\beta = 30$ corresponds to $\langle\theta\rangle \approx 15°$.

In order to realize substantial economies in computing time, it is desirable to perform the integration over θ in Eq. (A3) by approximate analytical methods. For the relatively large values of γ which characterize most of our films ($\gamma \geq 3.5$), this proves a relatively easy task since $\rho_1(\omega, k_\perp)$ is dominated by the leading $2d$ term which can be integrated to yield

$$I(V) = K \int_{-\infty}^{\infty} d\omega \, F(\omega, \omega', T) \rho_{CE}(\omega', 0) \times \mathrm{Re}\left(\frac{\rho_1(\omega, 0)}{1 - iy/\beta}\right), \tag{A7}$$

where $y = 2\pi c \Omega_1(\omega)$. [One notes that Eq. (A4) is regained in the limit as $\beta \to \infty$, that is, as $\langle\theta\rangle \to 0$.] Currents can now be computed as a function of bias by straightforward numerical integrations. Utilizing the five-point parabola method, subsequent numerical differentiations yield quiet and reliable derivatives dI/dV and d^2I/dV^2 which are then converted into the desired derivatives using standard identities. In instances where instrumental modulation broadening influenced our derivative measurements, computed derivatives have also been modulation averaged using sinusoid amplitudes equal to those of the experiment.

---

[1] A. F. Andreev, Zh. Eksp. Teor. Fiz. 46, 1823 (1964) [Sov. Phys. JETP 19, 1228 (1964)].

[2] W. J. Tomasch, Phys. Rev. Lett. 15, 672 (1965); 16, 16 (1966).

[3] W. L. McMillan and P. W. Anderson, Phys. Rev. Lett. 16, 85 (1966).

[4] W. J. Tomasch and T. Wolfram, Phys. Rev. Lett. 16, 352 (1966).

[5] T. Wolfram, Phys. Rev. 170, 481 (1968).

[6] Readers desiring a readable introduction to the general topic are referred to Ref. 5, Sec. I, II, and portions of IV.

[7] All non-Andreev scattering reduces level amplitudes and, hence, decreases the mfp parameter l_1. Abrupt changes in electronic properties near the M_1-M_2 interface may cause such scattering even under ideal circumstances, while metallurgical problems in this region may cause localized impurity scattering. Hence, values of l_1 inferred from normalized dV/dI amplitudes represent lower bounds for bulk impurity scattering.

[8] S. L. Colucci, W J. Tomasch, and Hyung Joon Lee, Phys. Rev. Lett. 32, 590 (1974).

[9] J. G. Adler and J. E. Jackson, Rev. Sci. Instrum. 37, 1049 (1966).

[10] B. L. Blackford and R. H. March, Can. J. Phys. 46, 141 (1968).

[11] B. L. Blackford, J. Low Temp. Phys. 23, 43 (1972).

[12] C. K. Campbell and D. G. Walmsley, Can. J. Phys. 45, 159 (1967). Film thicknesses were inferred from temperature-dependent film resistances and, although no specific thickness value was quoted for the film in question, context suggests a value greater than the bulk coherence length (~ 1.5 μm). No attempt appears to have been made to prevent tunneling from film edges.

[13] To facilitate comparisons with the gap measurements of Refs. 10 through 12, $V_B = (\Delta_{CE} + \Delta_1)/e$ is determined by the extrapolation method. See Fig. 1. Also, Δ_1 is approximated by $\frac{1}{2}eV_B$ whenever structure at $V_A = |\Delta_{CE} - \Delta_1|/e$ can not be resolved—a common occurrence.

[14] The parameter β is related to the rms tunneling angle $\langle\theta\rangle$ by $\langle\theta\rangle \simeq (2/\beta)^{1/2}$. See Appendix A.

[15] P. W. Wyatt, R. C. Barker, and A. Yelon, Phys. Rev. B 6, 4169 (1972).

[16] J. M. Rowell, W. L. McMillan, and R. C. Dynes (private communication).

[17] W. L. McMillan, Phys. Rev. 175, 559 (1968).

[18] The value $\beta = 30$ has been employed uniformly in all computations sensitive to the difference between $\beta = 30$ and $\beta = \infty$ ($k_\perp = 0$).

[19] J. G. Daunt, in *Progress in Low Temperature Physics*, edited by C. J. Gorter (North-Holland, Amsterdam, 1955), Vol. 1, p. 220.

[20] E. Fawcett, in *The Fermi Surface*, edited by W. A. Harrison and M. B. Webb (Wiley, New York, 1960), p. 197.

[21] J. R. Anderson and S. S. Lane, Phys. Rev. B 2, 298 (1970).

[22] P. B. Allen and M. L. Cohen, Phys. Rev. 187, 525 (1969).

[23] N. W. Ashcroft and J. W. Wilkins, Phys. Rev. Lett. 14, 285 (1965).

[24] W. L. McMillan, Phys. Rev. 167, 331 (1968).